Finite Element Modeling of Piaggio P.180 Aircraft for Noise Reduction Assessment

CARMEN BRANCACCIO[1,*], GIOVANNI FASULO[2], FELICIA PALMIERO[3], GIORGIO TRAVOSTINO[3], ROBERTO CITARELLA[1]

[1]Department of Industrial Engineering, University of Salerno,
Via Giovanni Paolo II, 132, Fisciano (SA),
ITALY

[2]Italian Aerospace Research Centre (CIRA),
Via Maiorise, 1, Capua (CE),
ITALY

[3]Piaggio Aerospace, Viale Generale Disegna, 1,
Villanova d'Albenga (SV),
ITALY

**Corresponding Author*

Abstract: This study presents the development of a high-fidelity coupled structural–acoustic finite element model of the Piaggio P.180 passenger cabin. The work aims to predict interior noise in the low- to mid-frequency range. To reduce computational cost, the fuselage was modeled using two-dimensional shell elements and one-dimensional beam elements. A detailed modal analysis accurately captured the cabin's resonance behavior: the first three structural modes showed good agreement with experimental data. Finally, harmonic response analyses were performed to evaluate the noise reduction through the airframe up to approximately 110 Hz.

Key-Words: Piaggio P.180; Aircraft Interior Noise; Finite Element Method; Noise Reduction; Modal Approach; Fluid-Structure Interaction.

Received: March 11, 2025. Revised: June 7, 2025. Accepted: July 8, 2025. Published: September 12, 2025.

1 Introduction

Improving the efficiency and safety of air transportation remains a primary goal for aircraft manufacturers. However, increasing market competition has made passenger comfort an equally critical factor, [1]. As a result, vibroacoustic performance is now considered as a key design requirement, necessitating coupled structural–acoustic analyses, [2]. Effective noise, vibration, and harshness (NVH) control begins with the identification of sources and transmission paths. Airframe vibrations, caused by engine, propeller and turbulent fluxes, produce structure-borne interior cabin noise. Engine noise characteristics vary by propulsion type: turbojets produce broadband jet noise, while turbofans exhibit tonal components due to the fan. Propeller and fan tones concentrate around blade-pass frequencies (BPF), overlaid onto broadband content, [3].

To address these complex vibroacoustic interactions, numerical methods such as the Finite Element Method (FEM), [4], Boundary Element Method (BEM) in its direct and indirect formulation, [5], and Isogeometric Analysis (IGA), [6], are commonly employed. In the mid to high frequency range, these deterministic approaches are often complemented by statistical or hybrid techniques to reduce computational burden, [7], [8].

Previous studies have proposed simplified fuselage representations for vibroacoustic modeling. In [9], a structural model based on stiffened shell theory was used to analyze structural and acoustic responses at the first harmonic of the blade-pass frequency. However, the fuselage was idealized as a cylindrical shell, limiting geometric accuracy. Similarly, in [10], a finite element-based method was employed to predict interior noise reduction at low frequencies dominated by propeller excitation. Again, a cylindrical approximation was adopted for the fuselage, introducing significant simplifications.

The present study overcomes such limitations by conducting a vibroacoustic analysis on a full-scale aircraft configuration, with the fuselage modeled in its entirety with detailed internal features and realistic sections. The high level of fidelity achieved enables meaningful validation through comparison with experimental data.

The full-scale, high-fidelity finite element model of the Piaggio P.180 — a distinctive turboprop executive/VIP light transport aircraft, [11], [12] — is described in Section 2. Results from the modal and frequency response analyses are presented in Section 3, while conclusions and future perspectives

are discussed in Section 4.

2 Finite element model of Piaggio P180

2.1 Coupled Vibroacoustic equations

For the vibroacustic problem, the objective is to determine $\boldsymbol{u}$, the displacement vector field in $\mathbb{R}^3$, and p, the pressure field in $\mathbb{R}$, satisfying structural equations in terms of dynamic equilibrium, boundary conditions, kinematic relationship and material constitutive equations. In the absence of external acoustic sources, acoustic pressure p satisfies Helmholtz equation:

$$\Delta p + \frac{\omega^2}{c_0^2} p = 0 \tag{1}$$

where ω denotes the pulsation and c_0 the speed of sound in the fluid. For more details see, [2].
The finite element discretization of both the structural and fluid domains allows for the introduction of the discretized fields $\mathbf{u}^h$ and p^h and the related virtual fields $\delta\mathbf{u}^h$ and δp^h:

$$\boldsymbol{u}^h = \mathbf{N}_s\mathbf{u} \quad \text{and} \quad \delta\boldsymbol{u}^h = \mathbf{N}_s\delta\mathbf{u} \tag{2}$$

$$p^h = \mathbf{N}_f\mathbf{p} \quad \text{and} \quad \delta p^h = \mathbf{N}_f\delta\mathbf{p} \tag{3}$$

where $\mathbf{N}_s$ and $\mathbf{N}_f$ are the FEM shape function and $\mathbf{u}$ and $\mathbf{p}$ the unknown vectors that represent the unknown nodal values.

By assembling the structural and acoustic governing equations together with the isoparametric discretization defined from Eqs. 2 and 3, the coupled vibroacoustic problem can be expressed in the matrix form:

$$\left(\begin{bmatrix} \mathbb{K} & -\mathbb{C} \\ \mathbf{0} & \mathbb{H} \end{bmatrix} - \omega^2 \begin{bmatrix} \mathbb{M} & \mathbf{0} \\ \rho_f\mathbb{C}^T & \mathbb{Q} \end{bmatrix}\right)\begin{bmatrix} \mathbf{u} \\ \mathbf{p} \end{bmatrix} = \begin{bmatrix} \mathbf{f} \\ \mathbf{0} \end{bmatrix} \tag{4}$$

Six operators are obtained: $\mathbb{K}$ Structural Stiffness Matrix, $\mathbb{M}$ Structural Mass Matrix, $\mathbb{C}$ Coupling Matrix, $\mathbf{f}$ External Structural Force, $\mathbb{H}$ Acoustic Stiffness Matrix, $\mathbb{Q}$ Acoustic Mass Matrix. By solving the problem with a modal approach, two eigenvalues problems - one for the structure and one for the acoustic cavity- must be solved (Eq. 5 - 6).

$$\left(\mathbb{K} - \omega^2\,\mathbb{M}\right)\boldsymbol{\varphi} = 0 \tag{5}$$

$$\left(\mathbb{H} - \omega^2\,\mathbb{Q}\right)\boldsymbol{\psi} = 0 \tag{6}$$

From the eigenvalue solution of the two decoupled systems, the eigenvectors $\boldsymbol{\phi}_s$ and $\boldsymbol{\phi}_f$ and eigenfrequencies ω_s and ω_f of the two systems are obtained. It is possible to pass from the Full Order Model (FOM) to the Reduced Order Model (ROM). The latter relies on the following assumptions:

$$\boldsymbol{u} \approx \boldsymbol{\phi}_s\,\boldsymbol{\alpha} \quad \text{and} \quad \boldsymbol{p} \approx \boldsymbol{\phi}_f\,\boldsymbol{\beta} \tag{7}$$

Substituting Eqs. 7 in Eq. 4 the reduced vibroacoustic problem is obtained in a fully coupled configuration and in the presence of external forces:

$$\left(\begin{bmatrix} \mathbb{K}_r & -\mathbb{C}_r \\ \mathbf{0} & \mathbb{H}_r \end{bmatrix} - \omega^2 \begin{bmatrix} \mathbb{M}_r & \mathbf{0} \\ \rho_f\mathbb{C}_r^T & \mathbb{Q}_r \end{bmatrix}\right)\begin{bmatrix} \boldsymbol{\alpha} \\ \boldsymbol{\beta} \end{bmatrix} = \begin{bmatrix} \boldsymbol{\phi}_s\mathbf{f} \\ \mathbf{0} \end{bmatrix} \tag{8}$$

where $\mathbb{M}_r$, $\mathbb{Q}_r$, $\mathbb{C}_r$, $\mathbb{K}_r$ and $\mathbb{H}_r$ are the reduced operators.

A more comprehensive derivation can be found in [2].

2.2 Structural Finite Element Model

To avoid the prohibitive cost of a modeling with solid elements, 3D thin-walled parts have been converted to equivalent 2D shells (CQUAD4 and CTRIA3). The Finite Element (FE) model includes six primary subsystems: external skin, circumferential frames, longitudinal stringers, bulkheads, cabin windows, and cabin floor, together with their local reinforcements. All of them, except the skin and bulkheads (omitted for clarity), are shown in Figure 1. The structural

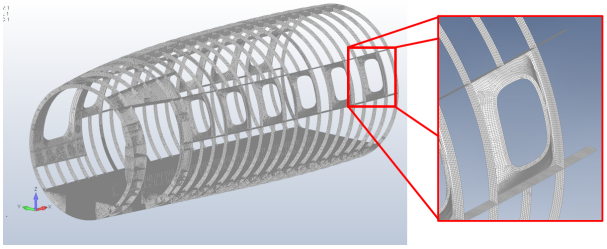

Fig. 1: FE representation of structural elements.
Source: created by the authors

mesh refinement is adequate for analyses aimed at quantifying the noise level up to the third BPF, which is approximately 500 Hz. A common meshing rule of thumb requires a structural model to capture natural modes accurately up to approximately 1.5–2 times the highest excitation frequency. Since the target analysis bandwidth is 500 Hz, the FE mesh was refined to remain reliable at least up to 800 Hz. Preliminary element sizing was guided by the closed-form expressions of [13], which provide analytical estimates for the natural frequencies of flat plates (see, [14]). The analytical natural frequencies is obtained by approximating the mode shape of each rectangular plate by the mode shape of single beams along the x and y axes. The analytical formulation

was used to identify the frequency f_{ij} closest to 800 Hz. The associated mode indices i and j define the highest vibration mode that must be resolved in the finite element model in the x and y directions, respectively. Finally, a characteristic element size was chosen so that a minimum of six elements span one bending wavelength at 800 Hz. For parts whose geometric complexity prevented analytical treatment, dedicated numerical mesh-convergence studies were conducted to ensure numerical accuracy.

2.3 Acoustic Finite Element Model

Since acoustic wavelength varies linearly with frequency, mesh sizing is governed directly by the relation:

$$\lambda = \frac{c}{f} \tag{9}$$

Considering a sound speed of c = 343 m/s, a maximum analysis frequency of 800 Hz, and enforcing ten linear elements (CTETRA4) per wavelength, the largest element edge length is roughly 42 mm. The acoustic mesh was matched to the structural mesh at the fluid–structure interface, ensuring nodal compatibility. Moving towards the central cavity volume, a transition zone allowed a gradual increase in acoustic element size, reaching the target mesh resolution within the cabin volume (see Figure 2).

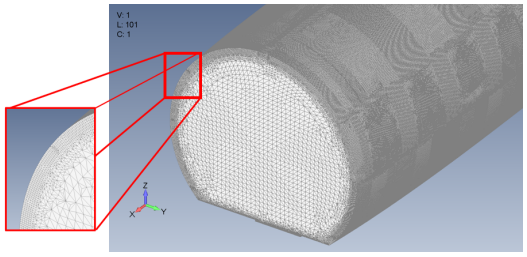

Fig. 2: Detail of the Acoustic FE model of P.180 cavities
Source: created by the authors

Considering both the structural and acoustic domains, this strategy enabled an accurate representation of the P.180 passenger cabin using approximately 17 million elements, of which 2 million represent the structural domain.

3 Results

3.1 Modal Analysis

A comprehensive modal analysis was carried out to assess the structural and acoustic natural frequencies. The structural model was assumed to be fully clamped at the fore and aft frames while the acoustic model was evaluated under rigid wall boundary conditions. Experimental testing, [15], was used to provide an empirical check on the structural behavior predicted by the numerical model. The end plates were omitted in the numerical model because, as installed during the test, they provided no structural stiffness. The numerical model was analyzed under ideal free–free boundary conditions. Experimental and numerical natural frequencies are compared in Table 1.

Table 1. Experimental VS. numerical (FEA) mode frequencies. The percentage difference is $|f_{\text{experimental}} - f_{\text{FEA}}|/f_{\text{experimental}} \times 100$.
Source: created by the authors

Mode	1	2	3
Experimental frequency [Hz]	32.7	36.5	66.2
FEA frequency [Hz]	25.5	31.9	74.6
Difference (%)	22.0	12.6	12.7

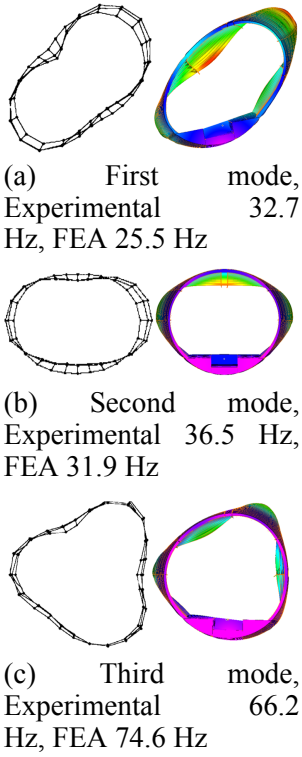

(a) First mode, Experimental 32.7 Hz, FEA 25.5 Hz

(b) Second mode, Experimental 36.5 Hz, FEA 31.9 Hz

(c) Third mode, Experimental 66.2 Hz, FEA 74.6 Hz

Fig. 3: Correlation between experimental and numerical (FEA) natural frequencies and their corresponding mode shapes
Source: Experimental data from [15]. numerical data created by the authors

While the test article comprised both the crew and passenger cabins, the FE model developed in the present study reproduces only the passenger cabin of the P.180. Consequently, the comparison must be regarded as qualitative: the first three computed

mode shapes correlate closely with the experimental results (Figure 3). In light of the modeling assumption previously outlined, the correlation between the results can be considered highly satisfactory.

3.2 Modal frequency response analysis

A forced, fully coupled, frequency response analysis, solved with modal approach at a set of discrete frequencies, was performed with an arbitrary spatially uniform and in phase acoustic excitation of 0.1 Pa, applied on the external fuselage surface skin. Representative boundary conditions were imposed by fully clamping the structure at its aft-most frames. The problem to be solved is described by Eq. 8.

Figure 7a and Figure 7b (A Appendix) present the total structural displacement and the acoustic pressure field, respectively, evaluated at the excitation frequency corresponding to the first acoustic cavity mode (37 Hz). Similarly, Figure 8a and Figure 8b (A Appendix) show the total structural displacement and the acoustic pressure field, respectively, evaluated at the excitation frequency corresponding to the first structural mode (87 Hz). As expected, the dynamic forced response of both cavity and structure is fully consistent with the corresponding cavity and structure excited natural mode. Minimum and maximum amplitude occur precisely at the predicted nodal and antinodal locations.

Finally, a two stage quantitative assessment of the cabin's acoustic insulation was conducted. First, at every passenger position, the frequency dependent modulus of the interior complex acoustic pressure $|p_{in}(f)|$ was calculated, under an acoustic pressure on the exterior surface $|p_{out}(f)|$ equal to 0.1 Pa at all frequencies. The cabin noise reduction (NR) spectrum was then obtained as:

$$\mathrm{NR}(f) = L_{\mathrm{out}}(f) - L_{\mathrm{in}}(f) \tag{10}$$

where $L_{\mathrm{out}}(f)$ and $L_{\mathrm{in}}(f)$ represent the exterior and interior sound pressure levels, evaluated for each discrete frequency within the 25 – 110 Hz band (consistently, the modal bases adopted included all the structural and acustic modes up to a frequency of 200 Hz).

Equation (10) reports, in decibels, the frequency-dependent attenuation provided by the airframe, i.e. the amount by which the structure dampens the incident acoustic pressure at every analyzed frequency.

Figure 4 presents the NR calculated at each passenger position (*Pax1-7*), together with the NR calculated using $p_{\mathrm{rms,avg}}(f)$, (see Eq. 11), in turn obtained by averaging the cavity sound field over a longitudinal cutting plane at the nominal ear height of seated occupants:

$$p_{\mathrm{rms},avg}(f) = \sqrt{\frac{1}{N}\sum_{i=1}^{N}\frac{|p_i(f)|^2}{2}} \tag{11}$$

where i denotes the set of nodes located on the cutting plane, and N is the total number of nodes on that plane at which the acoustic response was evaluated.

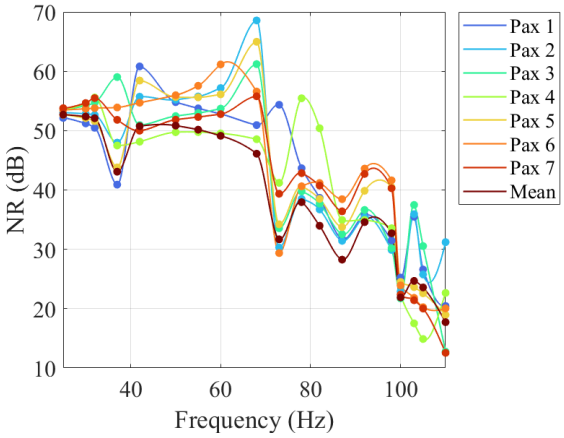

Fig. 4: Noise reduction
Source: created by the authors

An illustration of the passenger seating layout is provided in Figure 5 to enable accurate interpretation of the preceding graph.

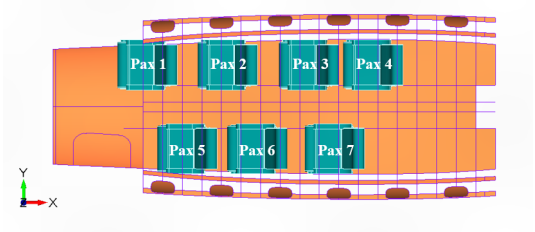

Fig. 5: Passenger seating layout
Source: created by the authors

Below approximately 87 Hz (first structural bending mode), the airframe panels operate in the stiffness-controlled region, and a gradual decay in noise reduction is expected as frequency increases. Superimposed on this trend are oscillations associated with the cabin's acoustic eigenmodes. All seating positions exhibit a marked NR local minimum, centered at about 37 Hz, that corresponds to the first global cabin acoustic resonance. However, seats 3, and, to a lesser extent, seats 6 and 7, are positioned near the pressure nodal plane of that mode and thus do not experience any attenuation of NR (see Figure 5, Figure 6).

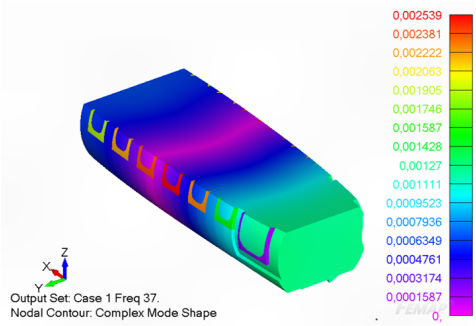

Fig. 6: Acoustic forced response contour, evaluated at a frequency corresponding to the first acoustic mode (37 Hz), on a plane at ear height
Source: created by the authors

A further local minimum in NR occurs near 73 Hz, coinciding with the second cabin acoustic eigenmode. At the first structural bending mode (87 Hz), all measurement locations exhibit a dip in NR, as the airframe resonance is excited almost uniformly throughout the cabin, with particularly pronounced effects at the window locations.

4 Conclusion

This study presents a high-fidelity yet computationally efficient structural-acoustic finite element model of the Piaggio P.180 aircraft, aimed at predicting cabin noise in the low- to mid-frequency band. Mesh sizing in both the structural and acoustic domains was guided by analytical wavelength estimates and numerical convergence studies, ensuring at least six elements per bending wavelength in the structure and ten elements per acoustic wavelength in the cabin air. A structural-acoustic modal analysis, when benchmarked against experimental modal data, confirmed that the coupled model reproduces the fundamental and higher-order eigenmodes of both the airframe and the cabin cavity within acceptable error margins. Experimental and numerical natural frequencies, for the first three modes, exhibited acceptable discrepancies, given the approximations inherent in the implemented boundary conditions and the absence of the crew cabin in the numerical model. The final harmonic response study, spanning 25 - 110 Hz, provided preliminary insights into P.180 fuselage noise reduction. Local minima in attenuation coincided with global acoustic resonances (37 Hz and 73 Hz) and with the first bending mode of the structure (87 Hz), while seat-specific variations reflected the nodal and antinodal distributions in the pressure field. The next step will involve the aerodynamic study of P.180 five blade propellers, in order to calculate the noise transmitted inside the fuselage from the first three BPF harmonics. This will allow assessment of the airframe's noise reduction properties under realistic flight conditions.

Declaration of Generative AI and AI-assisted Technologies in the Writing Process

The authors wrote, reviewed and edited the content as needed and verifies that none utilised artificial intelligence (AI) tools were used. The authors take full responsibility for the content of the publication.

References:

[1] S. Penning, J. Quehl, V. Rolny, Effects of aircraft cabin noise on passenger comfort, *Ergonomics*, 55:10, 1252-1265, 2012.

[2] H.J.-P. Morand, R. Ohayon, *Fluid-Structure Interaction: Applied Numerical Methods*, Wiley, 1995.

[3] D. Miljković, M. Maletić, M. Obad, Comparative investigation of aircraft interior noise properties, *Proceedings of the 3rd Congress of the Alps-Adria Acoustics Association, Graz, Austria*, 2007.

[4] T.J.R. Hughes, *The finite element method: linear static and dynamic finite element analysis*, Dover, 2000.

[5] S. Kirkup, The boundary element method in acoustics: A survey, *Applied Sciences*, 9(8), 1642, 2019.

[6] T. Landi, C. Hoareau, JF. Deü et al., Comparative vibroacoustic analyses: FEM vs. IGA, *Computational Mechanics*, 2025.

[7] A. Culla, W. D'Ambrogio, A. Fregolent, S. Milana, Vibroacoustic Optimization Using a Statistical Energy Analysis Model, *Journal of Sound and Vibration*, 375, 102-114, 2016.

[8] R. Gao, Y. Zhang, D. Kennedy, A hybrid boundary element-statistical energy analysis for the mid-frequency vibration of vibro-acoustic systems, *Comput. Struct.*, 203, 34-42, 2018.

[9] A. Grewal, D. Zimcik, R. Lapointe, Vibro-acoustic modelling in aircraft cabin noise transmission and control, *38th Structures, Structural Dynamics, and Materials Conference*, 8, 1997.

[10] G. Carducci, S. Carducci, Numerical Vibroacoustic Analysis of a Fuselage Section: Low-Frequency Noise Reduction, *PEGASUS-AIAA Student Conference*, 2019.

[11] A. Sollo, P. 180 Avanti: An Iconic Airplane and the Achievement of an Historical Milestone, *Aerotecnica Missili & Spazio*, 100, 69–78, 2021.

[12] R. de'Pompeis, P. Cinquetti, P. Martini, Development and Certification Flight Test on the Piaggio P. 180 Avanti Aircraft: A General Overview, SAE Technical Paper 911003, 1991.

[13] S. M. Dickinson, The buckling and frequency of flexural vibration of rectangular isotropic and orthotropic plates using Rayleigh's method, *Journal of Sound and Vibration*, 61(1), 1–8, 1978.

[14] R. Blevins, Formulas for natural frequency and mode shape, *Krieger Publishing Company*, 1995.

[15] T. Polito, F. Marulo, A. Sollo, M. Aversano G. Pagnozzi, Modal and acoustic characterization of structural components for fuselage applications, *In Proceedings of the 24th International Conference on Noise and Vibration Engineering (ISMA2010), Leuven*, 2010.

A Appendix

This appendix presents the forced response contour - specifically, the total structural displacement and the acoustic pressure field - evaluated at the excitation frequencies corresponding to the first acoustic cavity mode (37 Hz) and the first structural mode (87 Hz).

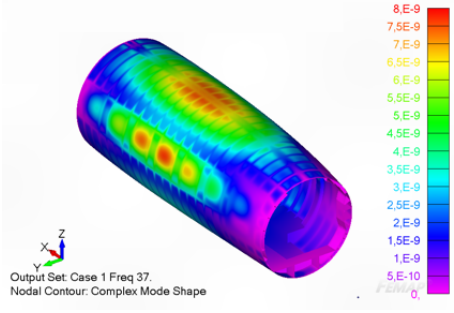

(a) Total displacement (m)

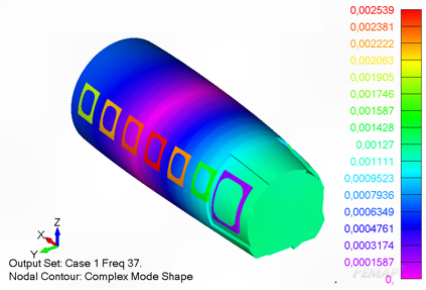

(b) Acoustic pressure (Pa)

Fig. 7: Forced response contour, evaluated at a frequency corresponding to the first acoustic cavity mode (37 Hz)
*Source: created by the author*s

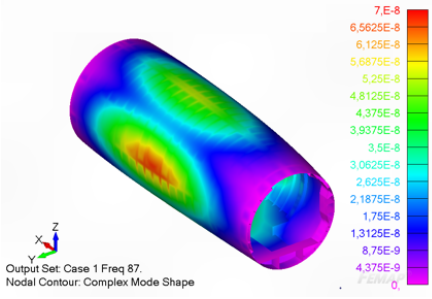

(a) Total displacement (m)

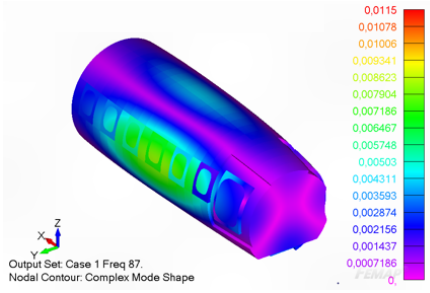

(b) Acoustic pressure (Pa)

Fig. 8: Forced response contour, evaluated at a frequency corresponding to the first structural mode (87 Hz)
Source: created by the authors

Contribution of Individual Authors to the Creation of a Scientific Article (Ghostwriting Policy)

Carmen Brancaccio was responsible for the development of the methodology, including the definition and implementation of the model. She performed the analyses, validated the results, and wrote the initial draft of the manuscript.
Giovanni Fasulo supported the definition of the modeling approach, managed the simulations on CIRA's workstations, and contributed to the writing of the manuscript.
Felicia Palmiero and Giorgio Travostino provided an initial 3D CAE reference model of the P.180 aircraft.
Roberto Citarella supervised the research activities and contributed to the refinement of both the methodology and the manuscript review process.

Sources of Funding for Research Presented in a Scientific Article or Scientific Article Itself

No funding was received for conducting this study.

Conflicts of Interest

The authors have no conflicts of interest to declare that are relevant to the content of this article.

Creative Commons Attribution License 4.0 (Attribution 4.0 International , CC BY 4.0)

This article is published under the terms of the Creative Commons Attribution License 4.0
https://creativecommons.org/licenses/by/4.0/deed.en_US